

Article

Insights into the Ligand Effect in β -CD@Fe₃O₄ Composites to Activate Peroxymonosulfate for Efficient Degradation of Pharmaceutical Contaminants: A Study Employing Density Functional Theory

Xi Quan, Pengzhao Lv, Linlin Yin, Wei Zuo, Yu Tian and Jun Zhang * 

State Key Laboratory of Urban Water Resource and Environment (SKLUWRE), School of Environment, Harbin Institute of Technology, Harbin 150090, China

* Correspondence: hitsunyboy@126.com; Tel./Fax: +86-451-8628-3077

Abstract: This study presents a detailed investigation into the use of β -cyclodextrin (β -CD) encapsulated iron oxide nanoparticle (β -CD@Fe₃O₄) composites, modified with different ligands, to activate peroxymonosulfate (PMS) for the degradation of pharmaceutical contaminants, namely, diclofenac, carbamazepine, and erythromycin. The focus is on understanding the ligand effect, particularly using citric acid (CIT), polyethyleneimine (PEI), and cetyl trimethyl ammonium bromide (CTAB), on the degradation performance of these composites. Employing density functional theory (DFT) calculations, this work examines the electronic structure and charge distributions of β -CD@Fe₃O₄ composites, providing insights into their interaction with various pollutants. The study reveals that the β -CD@PEI@Fe₃O₄ composite demonstrates superior degradation efficiency due to optimal electrostatic interactions, regardless of the pollutant's hydrophobicity. On the other hand, β -CD@CIT@Fe₃O₄ shows moderate efficiency, and β -CD@CTAB@Fe₃O₄ exhibits selective efficiency, particularly for hydrophobic compounds. These findings underscore the significant role of surface chemistry in modulating the activation of PMS and the degradation of contaminants, opening avenues for designing tailored β -CD composites for environmental remediation.



Citation: Quan, X.; Lv, P.; Yin, L.; Zuo, W.; Tian, Y.; Zhang, J. Insights into the Ligand Effect in β -CD@Fe₃O₄ Composites to Activate Peroxymonosulfate for Efficient Degradation of Pharmaceutical Contaminants: A Study Employing Density Functional Theory. *Coatings* **2024**, *14*, 439. <https://doi.org/10.3390/coatings14040439>

Academic Editor: Daniela Predoi

Received: 12 March 2024

Revised: 25 March 2024

Accepted: 7 April 2024

Published: 8 April 2024



Copyright: © 2024 by the authors. Licensee MDPI, Basel, Switzerland. This article is an open access article distributed under the terms and conditions of the Creative Commons Attribution (CC BY) license (<https://creativecommons.org/licenses/by/4.0/>).

Keywords: β -cyclodextrin; iron oxide nanoparticles; ligand effect; pharmaceutical contaminants degradation; peroxymonosulfate activation; density functional theory

1. Introduction

Pharmaceutical pollutants, now ubiquitously present in surface and groundwater, as well as in effluents and influents of wastewater treatment plants (WWTPs) and in sludge [1], pose significant ecological and health risks. The accumulation of these substances can lead to the decimation of wildlife populations, disrupt aquatic life's natural behaviors, and interfere with human endocrine systems [2]. It has been reported that diclofenac accumulates in various organs of fish at low concentrations (5 μ g/L) [3]. Additionally, a mixture of pharmaceuticals including carbamazepine at ng/L levels has been shown to inhibit the growth of human embryonic cells [4]. The biologically active properties of macrolide antibiotics such as erythromycin render them highly toxic to aquatic organisms [5]. Conventional WWTP treatments (primary, secondary, and tertiary) are often inadequate for fully removing diverse pharmaceuticals and their metabolites, presenting a formidable challenge in water quality management. This necessitates the development of more effective water-treatment technologies.

While alternative treatments like sedimentation, membrane bioreactors, and adsorption offer potential solutions for removing pharmaceutical contaminants, they are hampered by several factors. These include the low biodegradability of many pharmaceutical compounds, economic limitations, and issues with regeneration [6]. Advanced oxidation processes (AOPs) based on peroxymonosulfate (PMS) have emerged as promising alternatives,

capable of direct mineralization of contaminants in water. These processes generate reactive species with high redox potentials, such as sulfate radicals ($\text{SO}_4^{\bullet-}$, 2.5–3.1 V) and hydroxyl radicals ($\cdot\text{OH}$, 1.9–2.7 V), activated through heat, UV radiation, alkalinity, and metal ions [7]. Iron and its oxides, particularly rich in ferrous like Fe_3O_4 , are extensively studied catalysts, known for their efficiency, low toxicity, and cost-effectiveness [8]. However, the inherent magnetic properties and high surface energy of Fe_3O_4 lead to agglomeration, diminishing its catalytic performance.

Considering the remarkable physicochemical properties of many nanocomposite materials that have shown significant potential in water purification [9], along with the techniques involved in surface modification [10], a solution to this issue is the encapsulation of Fe_3O_4 nanoparticles with β -cyclodextrin (β -CD). This encapsulation results in the formation of a β -CD@ Fe_3O_4 nanocomposite which enhances its activation efficiency [11]. β -CD, composed of seven glucopyranose units, features hydrophilic outer layers and a hydrophobic cavity, which selectively adsorb pharmaceutical contaminants, forming host-guest inclusion complexes [12]. Moreover, β -CD's abundant hydroxyl groups allow for functionalization [11]. Yet, the role of ligands in β -CD@ Fe_3O_4 in organic contaminant removal remains under-explored.

This study aims to bridge this gap by thoroughly investigating the influence of these ligands on the efficacy of β -CD@ Fe_3O_4 nanoparticles in removing organic contaminants. Specifically, we compare the binding efficiency, stability, and contaminant removal capabilities of β -CD@ Fe_3O_4 linked with citric acid (CIT), polyethyleneimine (PEI), and cetyl trimethyl ammonium bromide (CTAB). The rationale behind selecting these three linking agents is based on their distinct functional properties and compatibility with β -CD. Citric acid, a tricarboxylic acid, offers multiple carboxyl groups that can chelate with iron oxide, enhancing the stability of the β -CD moiety on the nanoparticle surface. Polyethyleneimine provides a dense array of amine groups that can be protonated, thus introducing a positive charge to the nanoparticle surface, which is advantageous for adsorbing negatively charged contaminants. Lastly, cetyl trimethyl ammonium bromide, a quaternary ammonium compound, presents hydrophobic tail groups that can interact with the hydrophobic cavity of β -CD, potentially increasing the hydrophobic interactions with nonpolar contaminants. Through a combination of experimental analysis and theoretical modeling, we seek to elucidate the underlying mechanisms driving the performance variations observed with different ligand modifications. Our findings are expected to provide valuable insights into the design of more efficient and environmentally friendly nano-based remediation technologies for organic pollutant removal.

2. Experimental Section

2.1. Materials

β -cyclodextrin (β -CD), carboxymethyl- β -cyclodextrin, $\text{FeCl}_3 \cdot 6\text{H}_2\text{O}$, $\text{FeCl}_2 \cdot 4\text{H}_2\text{O}$, $\text{FeSO}_4 \cdot 7\text{H}_2\text{O}$, NaOH, ethylene glycol, anhydrous sodium acetate, polyethyleneimine (PEI), 1-ethyl-(3-dimethylaminopropyl) carbonyl diimide (EDC), 4-dimethylaminopyridine (DMAP), citric acid (CIT), isopropanol, cetyl trimethyl ammonium bromide (CTAB), ammonium hydroxide, diclofenac (DCF), erythromycin (ERY), and carbamazepine (CBZ) were purchased from Aladdin Chemistry Co., Ltd. (Shanghai, China).

2.2. Synthesis of β -CD@ Fe_3O_4 Linked with CIT, PEI, and CTAB

β -CD@PEI@ Fe_3O_4 , β -CD@CIT@ Fe_3O_4 , and β -CD@CTAB@ Fe_3O_4 were originally synthesized according to previous studies [13–15]. A detailed description of the synthesis protocols employed for the preparation of β -CD@ Fe_3O_4 composites can be found in the Supplementary Information (Text S1).

2.3. Experimental Procedures and Chemical Analysis

The degradation of three target PPCPs (diclofenac (DCF), carbamazepine (CBZ), and erythromycin (ERY)) was carried out individually in 100 mL bottles with magnetic stir-

ring. Specifically, the catalyst (5 mg) and PMS (5 mg) were successively dispersed into 50 mL, 20 mg/L of PPCP solution. Periodically, a 0.8 mL sample was taken, filtered, and quenched with 0.2 mL sodium thiosulfate pentahydrate ($\text{Na}_2\text{S}_2\text{O}_3 \cdot 5\text{H}_2\text{O}$, 0.02 M) in the sampling bottles.

High-performance liquid chromatography (HPLC, Agilent 1290, Santa Clara, CA, USA) with a diode array detector (DAD) and a C18 column ($150 \times 4.6 \text{ mm}$, $5 \mu\text{m}$) was used to determine contaminant concentrations. Detailed mobile phases are described in Table S1. The intermediates of DCF degradation were examined via high-resolution quadrupole time-of-flight mass spectrometry (Q-TOF/LC/MS, Agilent, GFEQ92313004, Santa Clara, CA, USA). The capillary voltage was set to 4000 V, the desolvation temperature was $350 \text{ }^\circ\text{C}$, the source temperature was $200 \text{ }^\circ\text{C}$, and the mass range was recorded from m/z 50–500.

2.4. Density Functional Theory (DFT) Calculations

In this investigation, simulations were conducted using ORCA 5.0.3 software, leveraging density functional theory (DFT) to ensure analytical precision. The RIJCOSX method was instrumental in expediting these calculations, balancing efficiency with accuracy. Optimal geometry and frequency calculations employed the B97-3c method, while ground-state energy assessments utilized the B3LYP functional in conjunction with a def2-TZVP(-f) basis set, broadening the analytical scope. DFT-D3(BJ) corrections were consistently applied across calculations to enhance accuracy. Additionally, the CPCM model was used to simulate water as the solvent, acknowledging the significance of environmental conditions in these simulations. This comprehensive methodology underscores the commitment to producing scientifically robust and replicable results, pivotal for advancing the field [16].

3. Results and Discussion

3.1. PMS Activation via $\beta\text{-CD@Fe}_3\text{O}_4$ towards DCF, CBZ and ERY Degradation

In this detailed examination of persulfate-based advanced oxidation processes (AOPs), we investigated the role of β -cyclodextrin-iron oxide composites ($\beta\text{-CD@PEI@Fe}_3\text{O}_4$, $\beta\text{-CD@CIT@Fe}_3\text{O}_4$, and $\beta\text{-CD@CTAB@Fe}_3\text{O}_4$) in the activation of persulfate (PMS) for the degradation of pollutants with varying hydrophobicity and hydrophilicity: diclofenac, carbamazepine, and erythromycin. As presented in Figure 1, over 90% degradation efficiency for DCF was achieved via the $\beta\text{-CD@PEI@Fe}_3\text{O}_4$ composite, which is posited to be due to the optimal electrostatic interactions facilitated by the dense array of amine groups in PEI, enhancing PMS activation irrespective of the hydrophilic or hydrophobic nature of the pollutants [17]. The efficient electron transfer processes induced by these groups potentiate the formation of sulfate radicals, which are the primary agents in the oxidation of both hydrophilic and hydrophobic organic structures [4]. In contrast, the $\beta\text{-CD@CIT@Fe}_3\text{O}_4$ composite exhibited moderate efficiency, potentially indicative of a more nuanced interplay between the hydrophilic citrate groups and the pollutants. The citrate moiety's interaction with hydrophobic pollutants like CBZ appears to be less favorable, perhaps due to the inherent water solubility and lower hydrophobic interaction capabilities of CIT, leading to a reduced activation of PMS and consequent degradation efficiency. Intriguingly, $\beta\text{-CD@CTAB@Fe}_3\text{O}_4$ showed a selective degradation profile, with a notably higher efficiency for ERY, a compound with significant hydrophobic regions. This suggests that the hydrophobic interactions between the CTAB's long alkyl chains and the hydrophobic domains of ERY may contribute to a more effective PMS activation and degradation process, as opposed to the hydrophilic DCF and moderately hydrophobic CBZ.

The differential degradation outcomes across the composites emphasize the intricate balance between hydrophobicity and the catalytic activation of PMS. Our results suggest that the interaction between the composite's surface chemistry and the pollutant's hydrophobic characteristics plays a critical role in the degradation process. This complexity not only demonstrates the importance of composite surface modification in optimizing AOPs but also highlights the need for a strategic approach to tackle pollutants with varying degrees of hydrophobicity in wastewater treatment processes. The insights gained from

this study could pave the way for the rational design of surface-modified β -cyclodextrin composites tailored to target specific pollutants based on their hydrophobic or hydrophilic properties, thereby enhancing the efficiency and specificity of AOPs in environmental cleanup endeavors.

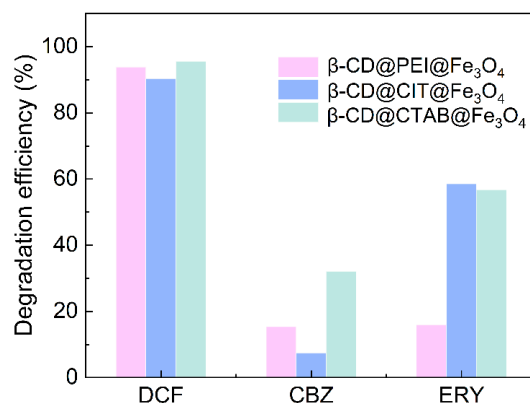


Figure 1. Comparative degradation efficiency of β -CD@CIT@Fe₃O₄, β -CD@PEI@Fe₃O₄, and β -CD@CTAB@Fe₃O₄ against DCF, CBZ, and ERY.

3.2. Electrostatic Properties of β -CD@Fe₃O₄ Nanocomposites

Mulliken charge analysis and electrostatic potential mappings of β -CD@Fe₃O₄ composites were investigated to unravel the interplay between structural design and functional efficacy. The β -CD@PEI@Fe₃O₄ complex, as illustrated in Figure 2a, showcases an array of amine groups, hypothesized to impart a high density of positive charges. These moieties are likely to engage in electrostatic interactions with negatively charged species, including PMS and certain pollutant molecules. One could postulate that the Mulliken charges on these amine groups would be significantly positive, contributing to a strong electrophilic character, which is expected to favor the activation of PMS and the generation of sulfate radicals for pollutant degradation. In Figure 2b, the β -CD@CIT@Fe₃O₄ complex is characterized by the presence of citrate ligands, which may present a multifaceted surface with both negative and positive regions. The carboxylate groups on citrate might confer a variable Mulliken charge distribution, resulting in diverse electrostatic potentials across the molecule. This heterogeneous charge distribution could influence the interaction with PMS and pollutants, leading to differential activation and degradation patterns. Lastly, the β -CD@CTAB@Fe₃O₄ complex depicted in Figure 2c features a long alkyl chain and a quaternary ammonium group, indicative of a hydrophobic domain coupled with a site of positive charge. This arrangement suggests a potential for hydrophobic interactions with pollutants possessing hydrophobic regions, which might align well with the long-chain structure of CTAB. The Mulliken charges are likely to be concentrated on the quaternary nitrogen, possibly facilitating interactions with electron-rich regions of pollutants and affecting PMS activation dynamics. Encapsulated within these conjectures lies the impetus for further computational and experimental investigations.

In this investigation, we meticulously analyzed the Mulliken charge distributions of β -CD@CIT@Fe₃O₄, β -CD@PEI@Fe₃O₄, and β -CD@CTAB@Fe₃O₄ nanocomposites, as well as their respective linkers CIT, PEI, and CTAB. The aim was to elucidate the influence of these charge distributions on the efficient removal of acidic, alkaline, and neutral pollutants. Figure 3 presents six histograms depicting the distributions of Mulliken charges across various chemical systems or conditions. Mulliken charges, derived from quantum chemical calculations, serve to quantify the charge distribution within molecules. The histograms indicate that the charge distributions for β -CD modified with citric acid and polyethyleneimine on iron oxide (Fe₃O₄) nanoparticles were approximately normal, centering around zero. In contrast, the β -CD modified with cetyltrimethylammonium bromide on Fe₃O₄ nanoparticles displayed a more peaked distribution, suggesting a predominant

charge state. CIT and PEI alone exhibited discrete sets of charge states, whereas CTAB alone presented two distinct peaks near -0.1 and 0.1 Mulliken charges, indicating two primary charge states. Overlaying the histograms, kernel density estimations (KDEs) smooth the discrete frequencies into a continuous curve, reflecting the probability density function of the variable [18].

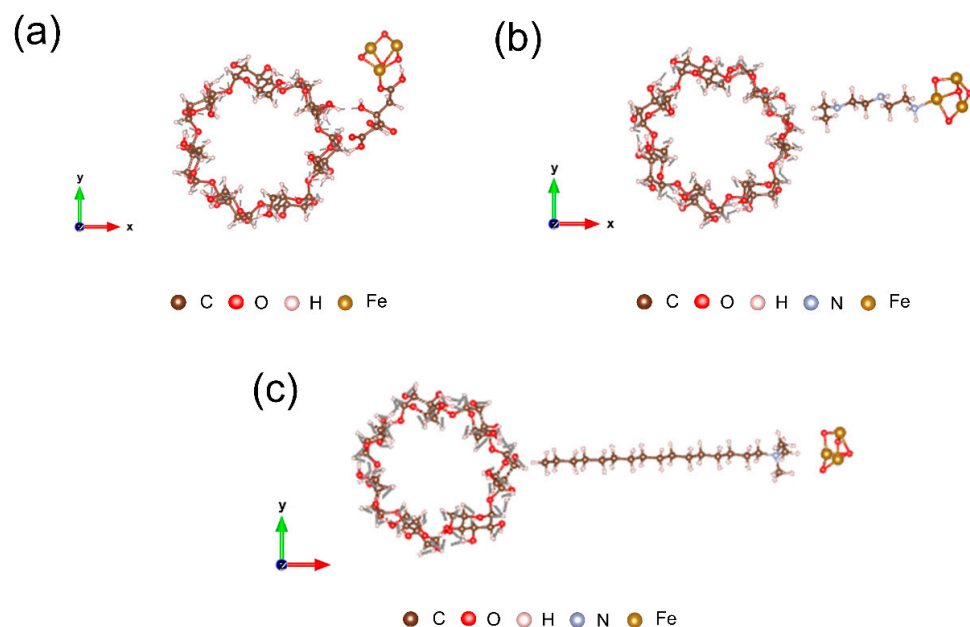


Figure 2. Schematic illustration of (a) β -CD@CIT@Fe₃O₄, (b) β -CD@PEI@Fe₃O₄, and (c) β -CD@CTAB@Fe₃O₄.

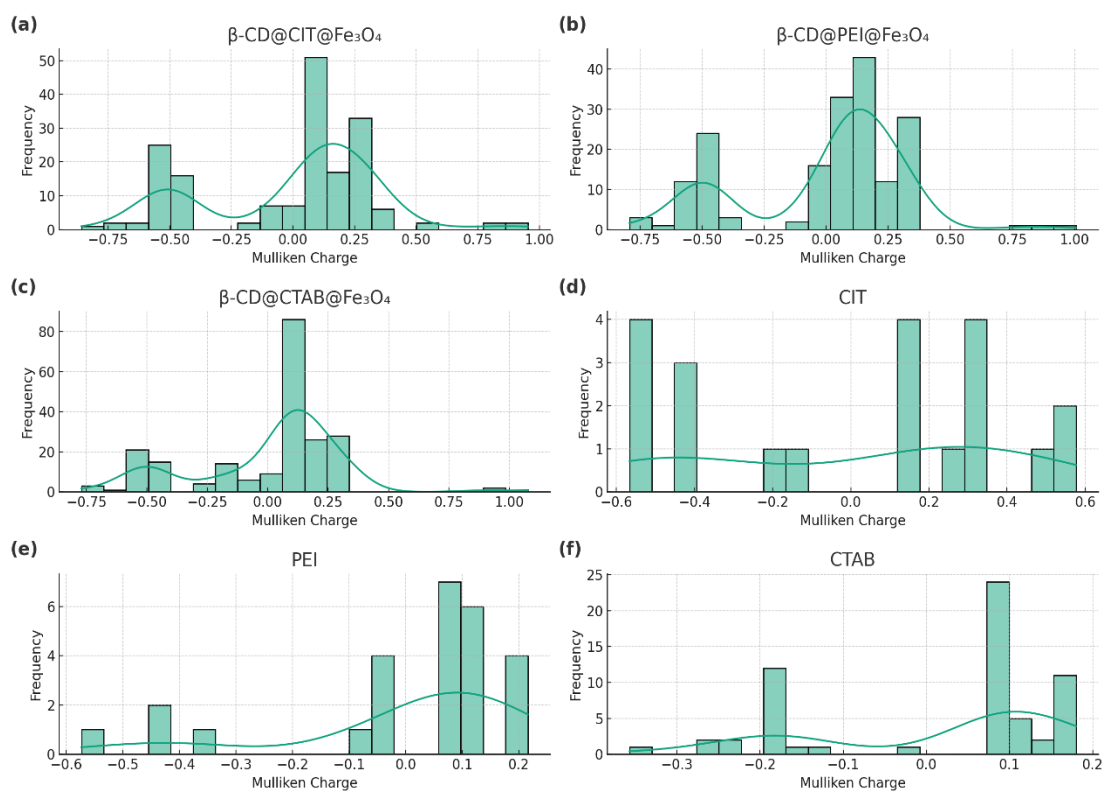


Figure 3. Histograms of Mulliken charges for (a) β -CD@CIT@Fe₃O₄, (b) β -CD@PEI@Fe₃O₄, (c) β -CD@CTAB@Fe₃O₄, (d) CIT, (e) PEI, and (f) CTAB.

An in-depth investigation of the electrostatic potential distribution characteristics was further conducted to reveal that the electrostatic properties imparted by the linkers significantly modulated the interaction of these nanocomposites with various pollutants. As displayed in Figure 4a, for β -CD@CIT@Fe₃O₄, the uniform charge distribution, primarily influenced by the CIT linker, suggests a balanced electrostatic environment. This characteristic is favorable for the adsorption of neutral pollutants, where charge neutrality plays a crucial role in interaction [19]. Furthermore, the moderate charge distribution endows this material with the versatility to interact with pollutants under a range of pH conditions, thus enhancing its application potential in diverse environmental settings [20]. In the case of β -CD@PEI@Fe₃O₄ (Figure 4b), the PEI linker imparts a distinct charge pattern, characterized by regions of high positive charges. This feature is particularly advantageous for the adsorption of negatively charged (anionic) pollutants typically found in alkaline environments. The enhanced electrostatic attraction in these regions could lead to improved capture efficiency for such pollutants [21]. Conversely, β -CD@CTAB@Fe₃O₄ in Figure 4c, influenced by the CTAB linker, exhibits a charge distribution that is conducive to the adsorption of positively charged (cationic) pollutants, commonly present in acidic environments. The higher negative charge regions within this material could favorably interact with these pollutants, facilitating their effective removal. These insights into the charge-dependent pollutant removal mechanisms underscore the significance of tailored charge engineering in cyclodextrin-based nanocomposites.

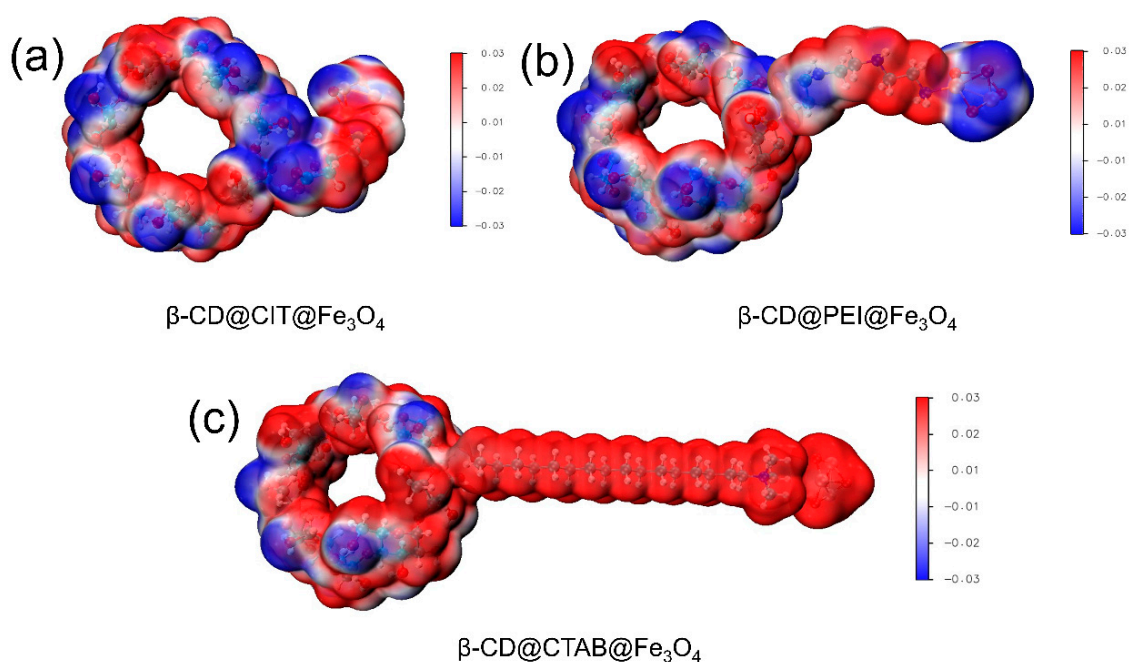


Figure 4. Molecular electrostatic potential surfaces for (a) β -CD@CIT@Fe₃O₄, (b) β -CD@PEI@Fe₃O₄, and (c) β -CD@CTAB@Fe₃O₄.

3.3. Molecular Dynamics and Electrostatic Potential Mapping of PMS Adsorption on β -CD@CTAB@Fe₃O₄

Building on the preliminary results discussed in Section 3.2, β -CD@CTAB@Fe₃O₄ was selected for further investigation due to its unique chemical properties and demonstrated effectiveness in contaminant adsorption and degradation, laying a solid foundation for a deeper exploration of its mechanisms and potential applications. In this study, we also meticulously investigated the adsorption configuration and charge density distribution of PMS on β -CD@CTAB@Fe₃O₄ nanoparticles, using advanced computational simulation techniques. Through molecular dynamics simulations, we acquired the three-dimensional coordinates and Mulliken charges of PMS molecules on the surface of the composite material. The results demonstrate a specific spatial arrangement of PMS molecules on the

material's surface, indicating strong interactions and potential orientation dependence with the substrate [22]. Observations from the side view (XZ plane) in Figure 5a and top view (XY plane) in Figure 5b reveal an uneven distribution of charge density between the PMS molecules and the surface of the β -CD@CTAB@Fe₃O₄ composite material. Particularly, significant variations in Mulliken charge values can be noted in certain areas, highlighting the uneven distribution of charges among the molecules, probably resulting from specific adsorption sites and interactions of PMS molecules on the material's surface.

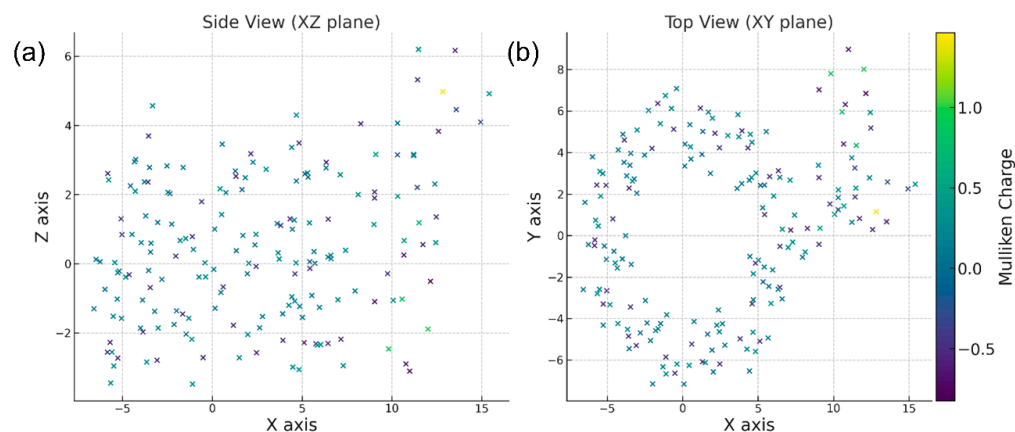


Figure 5. (a) Distribution of charge variations in β -CD@CTAB@Fe₃O₄ nanocomposites via side-view analysis; (b) Distribution of charge variations in β -CD@CTAB@Fe₃O₄ nanocomposites via top-view analysis.

Following the molecular dynamics insights, DFT calculations were employed to elucidate the adsorption-induced electrostatic potential landscape of PMS on β -CD@CTAB@Fe₃O₄ nanoparticles. The electrostatic potential map, as visualized in Figure 6, reveals a pronounced heterogeneity in charge distribution across the interface of the adsorbed PMS and the composite material. Regions of elevated positive potential (represented in red) interspersed with zones of negative potential (depicted in blue) are indicative of distinct areas of electron density accumulation and depletion, respectively. This dichotomy in charge polarization is indicative of the nuanced electrostatic environment created by the adsorption of PMS, which is a critical factor influencing the reactivity and stability of the adsorbed species [23]. The DFT-derived electrostatic potential map provides a quantum-level understanding of the adsorptive interactions, offering insights into the localized electronic environment that could govern the catalytic degradation pathways of PMS on the β -CD@CTAB@Fe₃O₄ surface. The intricate pattern of the potential distribution is a testament to the complex interplay between the PMS molecules and the functionalized magnetic nanoparticles, potentially leading to unique sites of enhanced catalytic activity due to the spatially varied electronic characteristics.

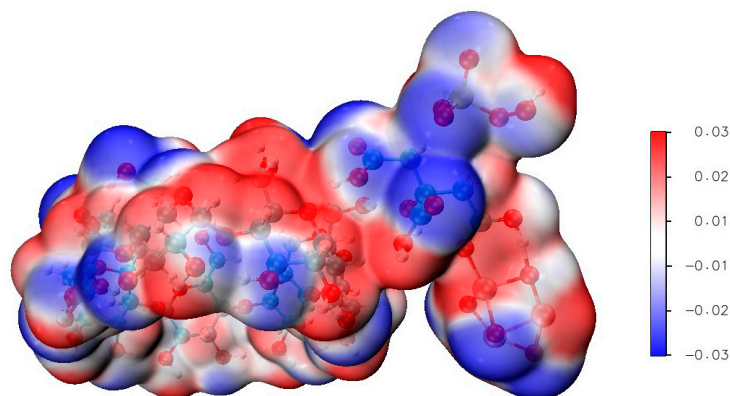


Figure 6. Molecular electrostatic potential map of PMS on β -CD@CTAB@Fe₃O₄ nanoparticles.

3.4. Electrostatic and Molecular Interactions in Pollutant Adsorption on β -CD@CTAB@Fe₃O₄

In this investigation, DFT calculations were utilized to elucidate the electrostatic potential landscapes governing the adsorption behavior of β -CD@CTAB@Fe₃O₄ towards CBZ, DCF, and ERY (Figure 7). The study reveals a nuanced interplay between the molecular structures and acid-base properties of the pollutants and the electrostatic features of the adsorbent surface. CBZ, a less polar molecule, exhibited moderate adsorption, largely governed by van der Waals and π - π interactions, minimally influenced by the surface's electrostatic potential (Figure 7a) [24]. DCF, in contrast, demonstrated pronounced adsorption efficiency, attributed primarily to its anionic nature which synergized with positively charged regions on the adsorbent (Figure 7b), indicating a strong electrostatic-driven adsorption mechanism [25]. ERY, with its large and complex structure, presents a challenging adsorption scenario (Figure 7c). Its diverse functional groups engaged in a multifaceted interaction pattern with the adsorbent, including electrostatic attractions and repulsions, hydrogen bonding, and steric hindrances, leading to a more complex and potentially less efficient adsorption process [26].

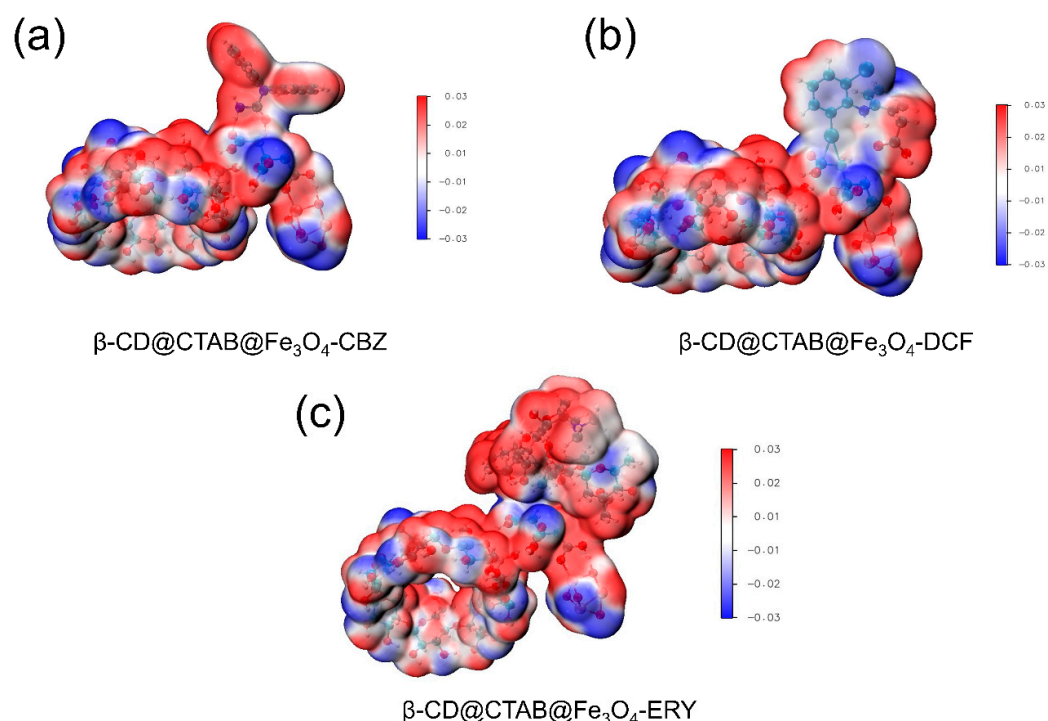


Figure 7. Molecular electrostatic potential of β -CD@CTAB@Fe₃O₄ complexes with (a) CBZ, (b) DCF, and (c) ERY.

3.5. Diclofenac Degradation Pathways in the β -CD@CTAB@Fe₃O₄/PMS System

In this comprehensive computational study, DFT calculations elucidated the intricate energy landscape underlying the oxidative degradation of DCF via the β -CD@CTAB@Fe₃O₄/PMS system predominantly involving hydroxyl groups (\cdot OH). The calculated potential energy profile reveals a sequential reaction pathway punctuated by a series of intermediates, each delineating the stepwise transformation of DCF in the presence of potent hydroxyl radicals generated from PMS activation (Figure 8). Initiation of the reaction pathway is characterized by the formation of the first intermediate (DP1), where the energy requirement (67.5 kcal/mol) suggests the surmounting of a significant activation barrier, probably involving the addition of \cdot OH to the DCF molecule or the abstraction of a hydrogen atom. This step is crucial as it primes the DCF molecule for subsequent degradation steps, which is consistent with the known reactivity of hydroxyl radicals towards aromatic compounds such as DCF. Progressing to DP2 and DP3, the endothermic nature of these steps, indicated

by the energy increments to 113.4 and 106.5 kcal/mol respectively, may be attributed to further hydroxylation reactions, leading to increased solubility and further breakdown of the aromatic system [27]. These processes are energetically demanding, potentially due to the disruption of resonance stabilization within the DCF molecule. The transition from DP3 to DP4 marks a thermodynamically favorable turn, as indicated by the substantial energy release to -79.8 kcal/mol. This transition is hypothesized to correspond to a critical bond cleavage, possibly the breaking of the aromatic ring or dechlorination, which are typically rate-limiting steps in the degradation of chlorinated aromatics. The observed energy release suggests that these reactions are exergonic and may lead to a rapid propagation of the degradation process once the initial energy barriers are overcome.

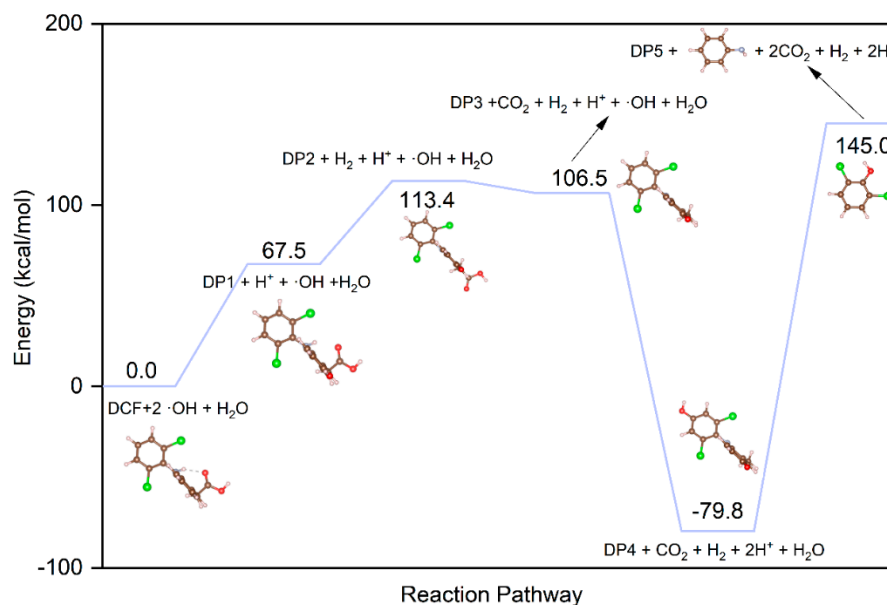


Figure 8. Diclofenac degradation pathways in β -CD@CTAB@Fe₃O₄/PMS system via \cdot OH.

The final step leading to the ultimate degradation products, including benzene, signifies a complete deconstruction of the DCF molecule, resulting in mineralization with the release of CO₂ and the formation of water. The peak at 145.0 kcal/mol prior to this step may represent the final energy-intensive process of breaking down persistent intermediates before achieving full mineralization. Several factors could influence this degradation pathway: (1) pH of the solution: the ionization state of DCF and the generation of \cdot OH radicals are pH-dependent, which can affect the rate and the pathway of degradation. (2) Concentration of PMS: higher concentrations of PMS can lead to a greater generation of \cdot OH radicals, potentially lowering the activation energy barriers. (3) Temperature: increased temperature can enhance the kinetics of the reaction, influencing the energy profile and the rate of degradation. (4) β -CD@CTAB@Fe₃O₄ surface properties: the catalytic surface characteristics, such as surface area, porosity, and charge distribution, directly impact the interaction with DCF and the activation of PMS. This potential energy profile, alongside a discussion on the influence of operational parameters, offers valuable insights into the optimization of the β -CD@CTAB@Fe₃O₄/PMS system for the degradation of chlorinated aromatic pollutants. It also provides a foundation for predicting the behavior of similar systems in the treatment of a wide array of persistent organic pollutants in wastewater treatment processes.

4. Conclusions

In conclusion, this study underscores the pivotal role of ligand modification in enhancing the efficiency of β -CD@Fe₃O₄ composites for pharmaceutical contaminant degradation through PMS activation. The use of different ligands, namely CIT, PEI, and CTAB, has been

shown to significantly influence the electrostatic and hydrophobic interactions between the composites and various pollutants. The β -CD@PEI@Fe₃O₄ composite emerges as a notably effective variant, facilitating high degradation efficiency across different types of pharmaceutical pollutants. This effectiveness is attributed to the dense array of amine groups in PEI, which enhance electrostatic interactions and promote efficient electron transfer processes. This study's findings on charge distribution and electrostatic potential characteristics provide crucial insights into the design of cyclodextrin-based nanocomposites for targeted pollutant removal. By tailoring the surface chemistry of these composites, it is possible to optimize the degradation process for a range of pollutants, significantly advancing the capabilities of advanced oxidation processes in environmental cleanup. This research not only contributes to a deeper understanding of the interactions between β -CD composites and pollutants but also paves the way for the development of more efficient and specialized materials for wastewater treatment and environmental remediation.

Supplementary Materials: The following supporting information can be downloaded at: <https://www.mdpi.com/article/10.3390/coatings14040439/s1>, Table S1. Molecular structures of organic compounds and HPLC settings.

Author Contributions: Conceptualization, X.Q.; Methodology, X.Q.; Formal analysis, P.L.; Resources, P.L.; Data curation, X.Q.; Writing—original draft, X.Q.; Supervision, L.Y., W.Z. and J.Z.; Project administration, Y.T. and J.Z. All authors have read and agreed to the published version of the manuscript.

Funding: This study was funded by the National Key R&D Program of China (2022YFC3801101), and National Natural Science Foundation of China (52170028).

Institutional Review Board Statement: Not applicable.

Informed Consent Statement: Not applicable.

Data Availability Statement: Data are contained within the article.

Acknowledgments: The authors appreciate the State Key Laboratory of Urban Water Resource and Environment, Harbin Institute of Technology (2023DX11), the Touyan Team and Heilongjiang Province S&T Program (HST2023GF003).

Conflicts of Interest: The authors declare that they have no known competing financial interests or personal relationships that may appear to influence the work reported in this paper.

References

1. Patel, M.; Kumar, R.; Kishor, K.; Mlsna, T.; Pittman, C.U., Jr.; Mohan., D. Pharmaceuticals of Emerging Concern in Aquatic Systems: Chemistry, Occurrence, Effects, and Removal Methods. *Chem. Rev.* **2019**, *119*, 3510–3673. [[CrossRef](#)]
2. Gadipelly, C.; Pérez-González, A.; Yadav, G.D.; Ortiz, I.; Ibáñez, R.; Rathod, V.K.; Marathe, K.V. Pharmaceutical Industry Wastewater: Review of the Technologies for Water Treatment and Reuse. *Ind. Eng. Chem. Res.* **2014**, *53*, 11571–11592. [[CrossRef](#)]
3. Koskue, V.; Monetti, J.; Rossi, N.; Nieradzick, L.; Freguía, S.; Kokko, M.; Ledezma, P. Fate of pharmaceuticals and PFASs during the electrochemical generation of a nitrogen-rich nutrient product from real reject water. *J. Environ. Chem. Eng.* **2022**, *10*, 107284. [[CrossRef](#)]
4. Rueda-Márquez, J.J.; Palacios-Villarreal, C.; Manzano, M.; Blanco, E.; del Solar, M.R.; Levchuk, I. Photocatalytic degradation of pharmaceutically active compounds (PhACs) in urban wastewater treatment plants effluents under controlled and natural solar irradiation using immobilized TiO₂. *Sol. Energy* **2020**, *208*, 480–492. [[CrossRef](#)]
5. Sendra, M.; Damián-Serrano, A.; Araújo, C.V.M.; Moreno-Garrido, I.; Blasco, J. Erythromycin sensitivity across different taxa of marine phytoplankton. A novel approach to sensitivity of microalgae and the evolutionary history of the 23S gene. *Aquat. Toxicol.* **2018**, *204*, 190–196. [[CrossRef](#)] [[PubMed](#)]
6. Wang, Y.; Wang, M.; Xie, Q.; Cai, X. Developments of cyclodextrin-coated Fe₃O₄@Fe⁰ nanoparticles to both efficiently activate persulfates and rapidly access hydrophobic PAHs in water. *Chem. Eng. J.* **2023**, *468*, 143510. [[CrossRef](#)]
7. Wang, J.; Wang, S. Activation of persulfate (PS) and peroxymonosulfate (PMS) and application for the degradation of emerging contaminants. *Chem. Eng. J.* **2018**, *334*, 1502–1517. [[CrossRef](#)]
8. Lu, J.; Zhou, Y.; Ling, L.; Zhou, Y. Enhanced activation of PMS by a novel Fenton-like composite Fe₃O₄/S-WO₃ for rapid chloroxylenol degradation. *Chem. Eng. J.* **2022**, *446*, 137067. [[CrossRef](#)] [[PubMed](#)]
9. Janjhi, F.A.; Ihsanullah, I.; Bilal, M.; Castro-Muñoz, R.; Boczkaj, G.; Gallucci, F. MXene-based materials for removal of antibiotics and heavy metals from wastewater—a review. *Water Resour. Ind.* **2023**, *29*, 100202. [[CrossRef](#)]

10. Vatanpour, V.; Yukselkadag, A.; Ağtaş, M.; Mehrabi, M.; Salehi, E.; Castro-Muñoz, R.; Koyuncu, I. Zeolitic imidazolate framework (ZIF-8) modified cellulose acetate NF membranes for potential water treatment application. *Carbohydr. Polym.* **2023**, *299*, 120230. [[CrossRef](#)]
11. Wu, G.; Tu, H.; Niu, F.; Lu, S.; Liu, Y.; Gao, K.; Chen, Z.; Wang, P.; Li, Z. Synthesis of polymer-functionalized β -cyclodextrin, Mg^{2+} doped, coating magnetic Fe_3O_4 nanoparticle carriers for penicillin G acylase immobilization. *Colloids Surf. A Physicochem. Eng. Asp.* **2023**, *657*, 130609. [[CrossRef](#)]
12. Qin, Y.; Ahmed, A.; Iqbal, S.; Usman, M. Construction of β -cyclodextrin modified Fe_3O_4 composites with enhanced peroxymonosulfate activation towards efficient degradation of norfloxacin. *Mol. Catal.* **2023**, *547*, 113368. [[CrossRef](#)]
13. Yan, H.; Yu, X.; Dong, G.; Zhang, Z.; Ding, K.; Yang, H.; Su, G. Functionalized β -cyclodextrin with polyethyleneimine-coated Fe_3O_4 as a recyclable demulsifier for the efficient treatment of oily wastewater. *Colloids Surf. A Physicochem. Eng. Asp.* **2023**, *660*, 130877. [[CrossRef](#)]
14. Jaina, Y.; Kumaria, M.; Agarwal, M.; Gupta, R. Robust synthesis of sugar-coumarin based fluorescent 1,4-disubstituted-1,2,3-triazoles using highly efficient recyclable citrate grafted β -cyclodextrin@magnetite nano phase transfer catalyst in aqueous media. *Carbohydr. Res.* **2019**, *482*, 107736. [[CrossRef](#)] [[PubMed](#)]
15. Sathyan, M.; Jandas, P.J.; Venkatesan, M.; Pillai, S.C.; John, H. Electrode material for high performance symmetric supercapacitors based on superparamagnetic Fe_3O_4 nanoparticles modified with cetyltrimethylammonium bromide. *Synth. Met.* **2022**, *287*, 117080. [[CrossRef](#)]
16. Lu, T.; Chen, F. Multiwfn: A multifunctional wavefunction analyzer. *Comput. Chem.* **2011**, *33*, 580–592. [[CrossRef](#)] [[PubMed](#)]
17. Ayalew, Z.M.; Guo, X.; Zhang, X. Synthesis and application of polyethyleneimine (PEI)-based composite/nanocomposite material for heavy metals removal from wastewater: A critical review. *J. Hazard. Mater. Adv.* **2022**, *8*, 100158. [[CrossRef](#)]
18. Zhang, J.; Cao, J.; Wu, T.; Huang, W.; Ma, T.; Zhou, X. A novel adaptive multi-scale Rényi transfer entropy based on kernel density estimation. *Chaos Solitons Fractals* **2023**, *175*, 113972. [[CrossRef](#)]
19. Miao, M.; Lu, Q.; Wang, X.; Zhang, Y.; Wong, N.H.; Sunarso, J.; Xiao, C.; Li, N. Removal of micro-organic contaminants from wastewater: A critical review of treatment technology. *Next Mater.* **2023**, *1*, 100016. [[CrossRef](#)]
20. Grape, E.S.; Chacón-García, A.J.; Rojas, S.; Pérez, Y.; Jaworski, A.; Nero, M.; Åhlén, M.; Martínez-Ahumada, E.; Feindt, A.E.G.; Pepillo, M.; et al. Removal of pharmaceutical pollutants from effluent by a plant-based metal-organic framework. *Nat. Water* **2023**, *1*, 433–442. [[CrossRef](#)]
21. Ahmed, M.; Mavukkandy, M.O.; Giwa, A.; Elektorowicz, M.; Katsou, E.; Khelifi, O.; Naddeo, V.; Hasan, S.W. Recent developments in hazardous pollutants removal from wastewater and water reuse within a circular economy. *npj Clean Water* **2022**, *5*, 12. [[CrossRef](#)]
22. Azhagiri, S.; Jayakumar, S.; Gunasekaran, S.; Srinivasan, S. Molecular structure, Mulliken charge, frontier molecular orbital and first hyperpolarizability analysis on 2-nitroaniline and 4-methoxy-2-nitroaniline using density functional theory. *Spectrochim. Acta Part A Mol. Biomol. Spectrosc.* **2014**, *124*, 199–202. [[CrossRef](#)] [[PubMed](#)]
23. Pan, Y.; Tang, L.; Ding, M. Electrostatic polarization in single-atom catalysis. *Cell Rep. Phys. Sci.* **2023**, *4*, 101417. [[CrossRef](#)]
24. Yu, Y.; Chen, D.; Xie, S.; Sun, Q.; Zhang, Z.-X.; Zeng, G. Adsorption behavior of carbamazepine on Zn-MOFs derived nanoporous carbons: Defect enhancement, role of N doping and adsorption mechanism. *J. Environ. Chem. Eng.* **2022**, *10*, 107660. [[CrossRef](#)]
25. Veclani, D.; Tolazzi, M.; Fogolari, F.; Melchior, A. Mechanism and thermodynamics of adsorption of diclofenac on graphene-based nanomaterials. *J. Environ. Chem. Eng.* **2022**, *10*, 108789. [[CrossRef](#)]
26. Albornoz, L.L.; da Silva, S.W.; Bortolozzi, J.P.; Banús, E.D.; Brussino, P.; Ulla, M.A.; Bernardes, A.M. Degradation and mineralization of erythromycin by heterogeneous photocatalysis using SnO_2 -doped TiO_2 structured catalysts: Activity and stability. *Chemosphere* **2021**, *268*, 128858. [[CrossRef](#)]
27. Long, H.; Chen, T.-S.; Song, J.; Zhu, S.; Xu, H.-C. Electrochemical aromatic C-H hydroxylation in continuous flow. *Nat. Commun.* **2022**, *13*, 3945. [[CrossRef](#)]

Disclaimer/Publisher's Note: The statements, opinions and data contained in all publications are solely those of the individual author(s) and contributor(s) and not of MDPI and/or the editor(s). MDPI and/or the editor(s) disclaim responsibility for any injury to people or property resulting from any ideas, methods, instructions or products referred to in the content.